Skin Modeling Analysis of a Force Sensing Instrument-Assisted Soft Tissue Manipulation Device

Ahmed M. Alotaibi
School of Mechanical Engineering,
Purdue University,
West Lafayette, IN 47907
e-mail: alotaib3@purdue.edu

Sohel Anwar[1]
Mem. ASME
Department of Mechanical and Energy Engineering,
IUPUI,
Indianapolis, IN 46202
e-mail: soanwar@iupui.edu

M. Terry Loghmani
School of Health and Rehabilitation Sciences,
IUPUI,
Indianapolis, IN 46202
e-mail: mloghman@iu.edu

Instrument-assisted soft tissue manipulation (IASTM) is a form of manual therapy which is performed with rigid cast tools. The applied force during the IASTM process has not been quantified or regulated. Nor have the angle of treatment and strokes frequency been quantified which contribute to the overall recovery process. This paper presents a skin modeling analysis used in the design of a novel mechatronic device that measures force in an IASTM application with localized pressures, similar to traditional, nonmechatronic IASTM devices that are frequently used to treat soft tissue dysfunctions. Thus, quantifiable soft tissue manipulation (QSTM) represents an advancement in IASTM. The innovative mechatronic QSTM device is based on one-dimensional (1D) compression load cells, where only four compression force sensors are needed to quantify all force components in three-dimensional (3D) space. Here, such a novel QSTM mechatronics device is simulated, analyzed, and investigated using finite element analysis (FEA). A simplified human arm was modeled to investigate the relationship between the measured component forces, the applied force, and the stress and strain distribution on the skin surface to validate the capability of the QSTM instrument. The results show that the QSTM instrument as designed is able to correlate the measured force components to the applied tool-tip force in a straight movement on the skin model. [DOI: 10.1115/1.4039661]

Introduction

Instrument-assisted soft tissue manipulation (IASTM) is a physical therapeutic intervention that employs a solid device to apply certain amounts of force to mobilize injured and/or restricted tissue with therapeutic benefit. Soft tissue manipulation (STM), i.e., massage, whether by hand alone or with a device, has been utilized widely for millennia to treat soft tissue dysfunction; however, the absence of force measurements has limited the development of its optimal dosing [1–3]. In IASTM treatments, applying a pressure to an area of extreme scar tissue or fibrosis using a solid tool has been found to be beneficial to patients [1–10]. These treatments helped to expedite the healing and restructuring of affected tissue for a multitude musculoskeletal conditions throughout different regions of the body in animals and humans. Different advantages and benefits under various circumstances and tissues were achieved using IASTM, including decreased pain and improved functional mobility. However, more studies and investigations are needed to comprehend the IASTM mechanisms and optimization [4–18].[2]

The STM dose-frequency has been studied in the literature [3,19–21]. However, due to the absence of accurate measurement methods for the STM movement and applied pressure to patients, these studies do not adequately report dose-pressure relations in human soft tissue [5,17,22–27]. Other treatment forms, such as ultrasound, electrical stimulation, and traction, have different critical parameters that need to be measured accurately. However, the attributes of the STM assessment and progress are based on the practitioners' subjective qualifications and judgment. Various studies have tried to quantify the applied force during the IASTM utilizing different methodologies, but none with clinically applicable, real-time device systems or methods [5].

A study conducted by Lee et al. [17] analyzed how flexeor carpi radialis motoneuron pool excitability was affected by transferred friction massage in human subject. The massage frequency, transitory pressure, and total resultant pressure were measured using an ultrathin flexible pressure sensor (ConTacts C500) built in the thumb of a plastic glove. However, this system could potentially result in inexact pressure measurements due to hand slippage inside the glove, electric shock hazard, and therapists' thumb sizes and softness. The slippage and frictional between the therapist and the glove could lead to false force measurements. Any tears in the glove could lead to an electric shock for patients or physicians. Thumb stiffness would introduce a critical parameter during force measurements and need to be studied.

A study conducted by Wang et al. [18] used a computerized system developed to produce a compression or transverse force using feedback system. The device was based on a base and two movable axes to apply forces in the horizontal X and vertical Z axes. The base was used to hold the subject, such as rats and rabbits. Two piezo resistance force sensors, which attached bellow the Z-axis, were used to quantify both force measurements in the X and Z directions. Various device tips, which could be attached to the sensors, were manufactured using stainless steel to target different types of tissue size. This large system has been shown to be a good methodology to measure the applied force. However, the system is not clinically applicable for human study, because of the complexity, lack of maneuverability, and involved setup.

Another animal study by Zeng et al. [26] built an automated compression system based on a pneumatic system. The device was designed to apply a given pressure on a rabbit using a linear motion control. A force transducer (Pasco, Inc., Philadelphia, PA) was used to provide the feedback signal to the device system. In contrast, in real practice, the tool should be portable, able to perform repeatable measurements, and relevant to clinical application.

The lack of quantifiable soft tissue manipulation (QSTM) poses a significant gap in STM practice. Thus, an urgent need exists for QSTM to support evidence-based practice leading to improved outcomes. In order to close this gap, the purpose of this research paper is to present, analyze, and evaluate a novel mechatronic QSTM device system for force sensing of localized pressure application using a skin modeling approach. The treatment tip of the QSTM device is similar to a commercially available, standard

[1]Corresponding author.
[2]http://www.grastontechnique.com

Manuscript received November 26, 2017; final manuscript received March 9, 2018; published online April 26, 2018. Assoc. Editor: Ning An.

Fig. 1 GT-3 treatment tip[2]

(nonmechatronic) IASTM device (Graston Technique®'s GT-3, Indianapolis, IN) (Fig. 1) used for localized treatment. The innovative QSTM device utilized one-dimensional (1D) compression load cells; four force sensors were considered to quantify the three force components on the skin surface in the three-dimensional (3D) space. The main goal of this study was to model, manufacture, and analyze a new device, which can measure all force components accurately. In addition, the new device can provide the users with other important parameters during the IASTM, e.g., the device's orientation in 3D space and stroke frequency. In addition, a real time user friendly interface with all measurements was implemented. The selected design and determined number of load cells will be used for future, ongoing development design concepts intended for extension to other devices' tip styles based on the tissue condition and type. In this computational study, the objective is to evaluate the stress and strain levels induced on a simplified skin model with respect to the applied hand pressure and the resulting force/stress levels at the load cell locations.

The Quantifiable Soft Tissue Manipulation Device Design and Analysis

Design Requirements. Different requirements were considered in designing the QSTM device. It should be operated using minimum voltage to minimize the hazard of electric shock. The system should be light, small, durable, and movable. The expected force range 0–150 N should be measured. In addition, device orientation, strokes frequency should be quantified. It is favorable that the new system can be applied to different QSTM tools. It should be affordable. Finally, a user friendly interface screen is needed to provide students, researchers, and physicians with all treatment information simultaneously.

Electronics Selection. Broad investigation and analyses have been carried on to achieve the best device which would meet all design requirements. To quantify the angles and stroke frequency, the IMUduino microcontroller [27] was chosen. The IMUduino had Gyroscope, a Compass IC, and an accelerometer. Also, it was the smallest powerful Arduino-based microcontroller with a dimension of 39.8 mm × 15.72 mm which resulted in a smaller size device.

After a comprehensive search on finding the suitable force sensors for the QSTM device, the FC-08 [21] one-dimensional compression load cell was chosen. It was manufactured by Forsentek Co., Limited, as shown in Fig. 2. It had the ability to quantify forces up to 20 kg of force that applied to its mesa. The dimension of the sensor was 8 mm diameter and 5 mm height. The signal of the load cell needs to be filtered and amplified before force mapping and calibration. Signal conditioning was needed for signal amplification.

The Quantifiable Soft Tissue Manipulation Design. After all electrical components had been chosen, the new QSTM device was

Fig. 2 The compression load cell (FC-08™) [28]

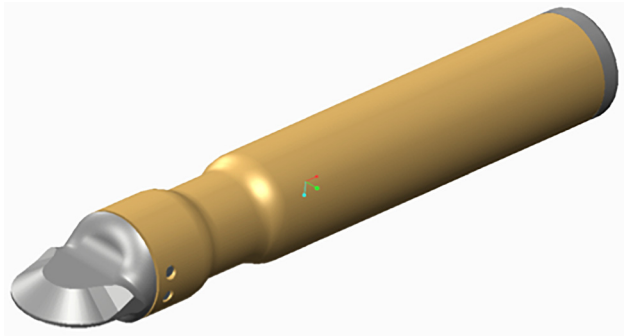

Fig. 3 CAD model of the QSTM device

designed using CAD software (Creo 2.0™). This design was built to accommodate the selected electronics and forces sensor, as shown in Fig. 3. The QSTM device model includes device tip, body, back cover, and keyways. The model's tip was made to mimic the GT3™ tip, and the purpose was to have the same for aiming soft tissues. An internal front cavity was included to accommodate the four load cells (Fig. 4(*a*)). In addition, a rear chamber was made to accommodate the electronics that is needed to run the device. In terms of insulation, the back cover was designed to secure and isolate the electronics inside the back chamber. The body of the device was tapered near the front of the device to allow for a panicle grip hand position.

In terms of sensor placements, four force sensors were used to quantify the three force components in the *X*, *Y*, and *Z* directions. The IASTM device orientations were considered because different treatment angles needed to be taken into consideration. Based on the real practice of IASTM, the new device expected to be tilted within the angles of 20 to 70 degrees with respect to the skin surface in a regular treatment. In this study, the *X*–*Y* plane represented a skin surface, and the QSTM device was rotated about the *Z* axis, which was the normal to the skin surface. A force analysis was conducted based on constraints, the force sensors were distributed inside the force measurement's cavity, as shown in Fig. 4(*b*).

The force measurements of the load cells were varied based on the orientation of the device and the load cells positons, as shown in Fig. 5. Three different scenarios were expected and analyzed.

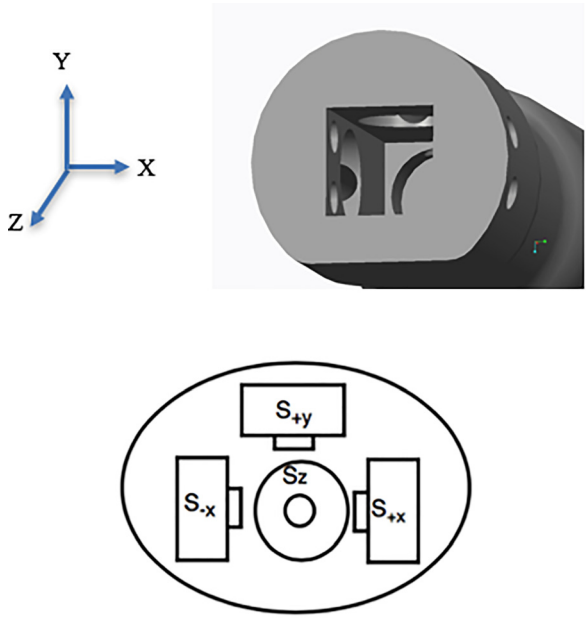

Fig. 4 (*a*) Sensor placements in the front cavity of the QSTM device and (*b*) the force sensor placement inside the device measurement cavity

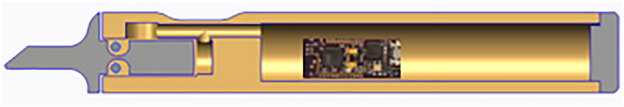

Fig. 5 Full sectional view of the QSTM device

When force was applied vertically at the QSTM device's head, the load cells S_{z+} and S_{y+} would quantify force measurements based on the device angle to the skin surface. The S_{z+}, S_{x-}, and S_{y+} load cells would quantify forces when force was applied within an angle 0 to 89 deg to the device's tip. When force applied within an angle 91 and 180 deg to the QSTM device's head, the load cells S_{z+}, S_{x+}, and S_{y+} would quantify the force components. According to the force analysis, there were no need for the fifth force sensor in the direction of $-Y$, because there would not be a force component on that direction based on the analysis. This would reduce the cost of the final device.

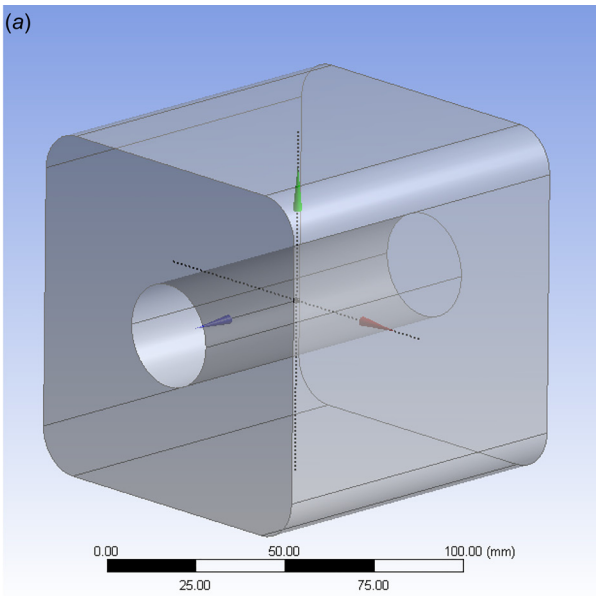

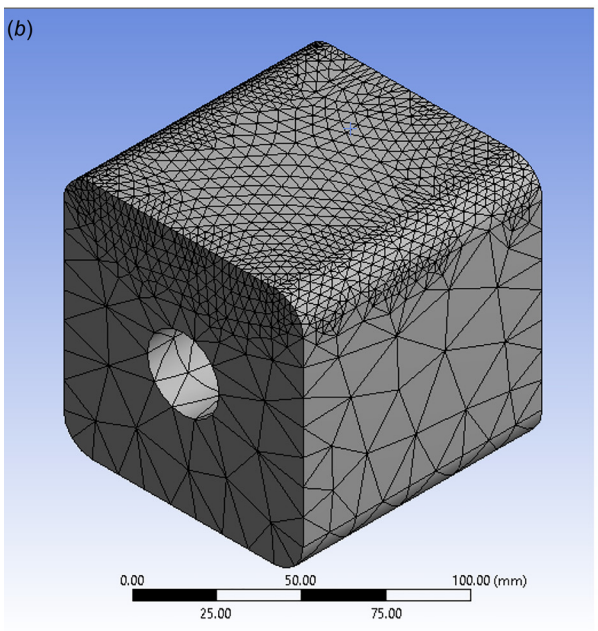

Fig. 6 (*a*) Human arm model in ANSYS and (*b*) skin arm meshing

Table 1 Selected mechanical properties for the arm model

Parameter	Value
Element type	3D solid quadrilateral isotropic
Density	1050 kg/m^3
Young's modulus	0.82 MPa
Poisson's ratio	0.48
UTS	12.6 MPa

UTS: ultimate tensile strength.

As shown in Fig. 5, the applied force to the device's head was transferred to the force sensors, which would convey the measurements data to the microprocessor using very thin wires. Very tiny wiring canals were utilized to allow for sensors connections. Force transformation was performed based on the device's orientation. The two keyways were used to connect the tip to the device's body with clearance of 3 mm, so it would not interfere with transferred forces.

Analysis of the Proposed Device Design Skin and Tissue Modeling. Human soft tissue is a complicated structure, which consists of different layers, such as skin, subcutaneous adipose tissue, fascia, and muscle, down to the bone, where each one has its

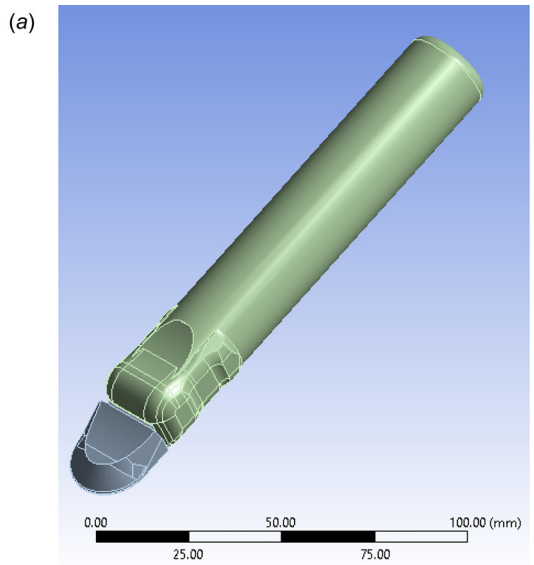

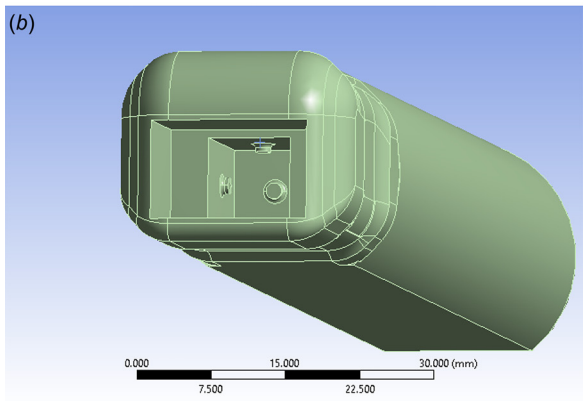

Fig. 7 (*a*) Quantifiable soft tissue manipulation device model in ANSYS and (*b*) the four load cells embedded into the front cavity of the QSTM device

Table 2 Mechanical properties of the QSTM device model

Parameter	Value
Density	7750 kg/m^3
Young's modulus	1.93×10^5 MPa
Poisson's ratio	0.31
UTS	586 MPa

own mechanical characteristics. In this study, a human arm was selected to be cube with 100 mm per side, where four filet edges were constructed to have the side curvatures, as shown in Fig. 6(*a*). Also, a bone placement was simulated as a hollow cylinder with a diameter of 30 mm. Then, the arm model was transformed to ANSYS WORKBENCH R15.0.

In this preliminary study, it was assumed that the maximum value of the skin mechanical properties found in Refs. [29–32] is representative of the skin model as it would reflect the combined characteristics of skin and underlying muscle. Agache et al. [29] studied and analyzed the mechanical characteristic of the human skin and found Young's modulus varied between 0.42 MPa and 0.85 MPa in vivo. The skin density was estimated to be about 1050 kg/m^{-3} [30]. Using the indentation test, Poisson's ratio was found to be 0.48 [31]. The ultimate tensile strength (UTS) of all tissue layers was found to be varied between 5.7 and 12.6 MPa [32]. Table 1 shows the selected mechanical properties for the arm model.

After the mechanical properties of the skin model were selected, the arm model was meshed, as shown in Fig. 6(*b*). Meshing was performed to investigate the stress and strain distribution on the skin surface. Meshing affects both the solution accuracy and the solving time. More mesh would result in more solving time but more accurate results and vice versa. Therefore, mesh refinement was used to the top of the skin model because the main goal was to investigate the skin reaction to the hand force using the QSTM device.

The Quantifiable Soft Tissue Manipulation Device Modeling. ANSYS WORKBENCH R15.0 was used to conduct the simulation and the QSTM device model was imported, as shown in Fig. 7(*a*). Both the device and the body of the device were defined to be stainless steel with specific mechanical properties, as shown in Table 2. Stainless steel was selected because of its high stiffness properties as compared to the other materials used in an IASTM. Some assumptions had been considered during the simulation to make the simulation and investigation easier. The back cover was assigned to be welded to the QSTM device's main body. The four

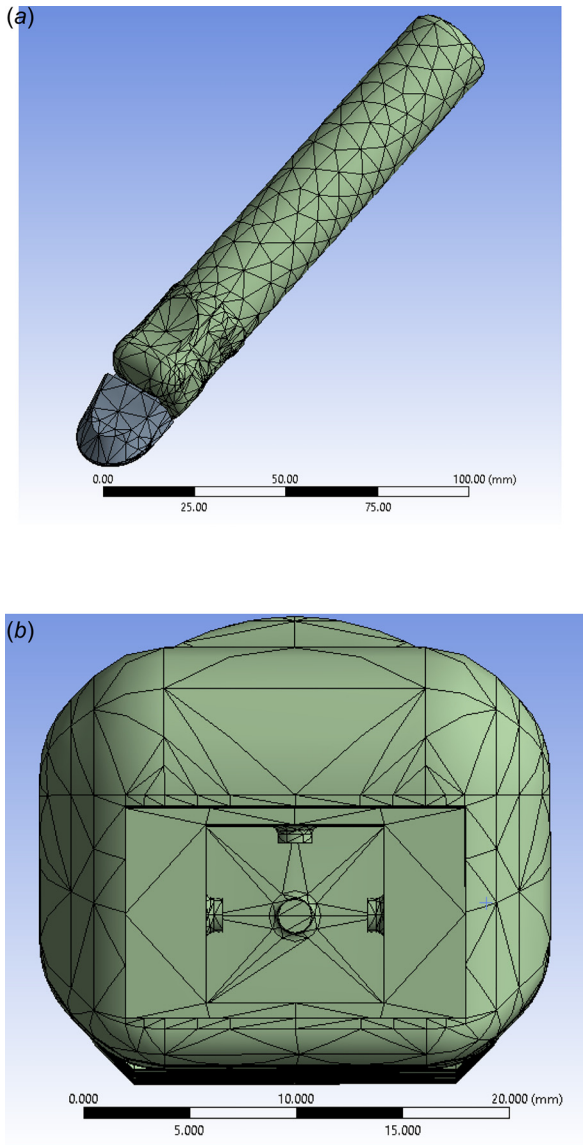

Fig. 8 (*a*) Meshed QSTM device and (*b*) meshed load cells in ANSYS

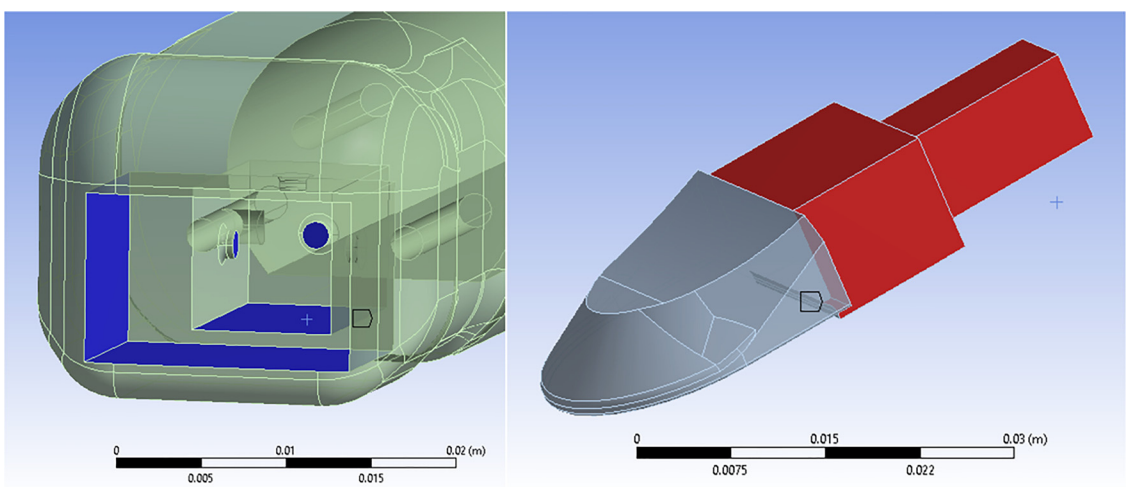

Fig. 9 Device tail and tip for bonded connections

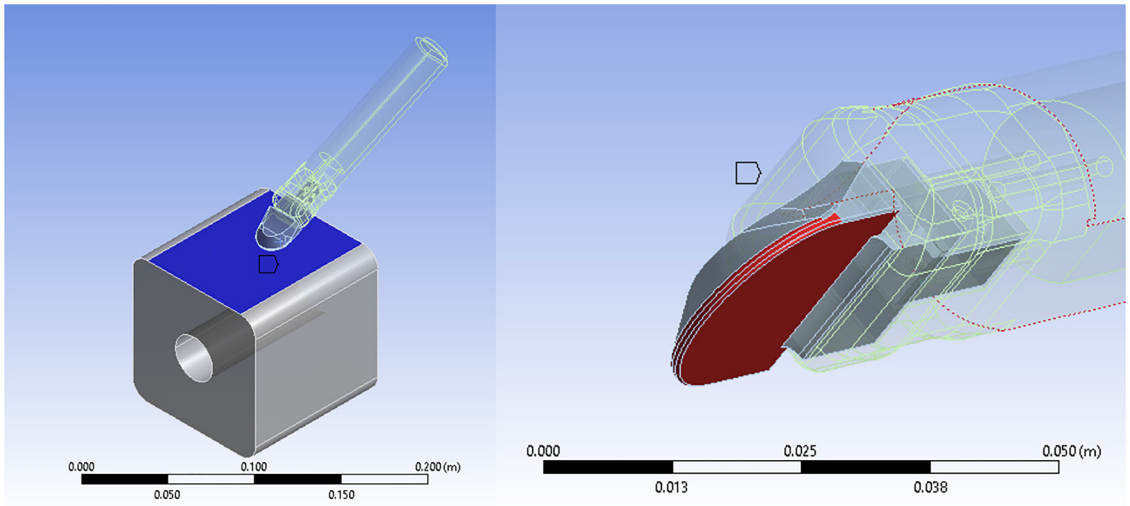

Fig. 10 Device tip and skin bonded contact areas in ANSYS

stainless steel force sensors were immersed into the device's main body, as shown in Fig. 7(*b*).

The complete device model was imported to ANSYS, then meshing was performed. Meshing was refined for both load cells' tips and the QSTM device's tip. As a result, accurate results were expected to be achieved, as shown in Figs. 8(*a*) and 8(*b*).

Simulation Setup. The simulation constraints, such as bonds and the structural settings, were assigned before moving to the simulation stage. Depending on the type of connection between the device's head and the skin model, bonded and frictional scenarios were studied using ANSYS. In both scenarios, the angle between the QSTM device and the arm model was selected to be 20 deg.

Bonded Contact Between the Tip and the Skin. When hand pressure was applied to the back cover of the device, reaction forces would be measured on the device's tip. The force measurements were conveyed back to the four load cell's tip through the device's tip, which is connected to the device's body with small tolerance. For the first scenario, the device's tip and the device's body were considered bonded, that means they were glued together. Nine faces were selected on both device's tip and body to be the contact areas, as shown in Fig. 9.

In addition, the relationship between the device's head and the skin model was defined as a bonded connection. This assumption was made to investigate the momentary applied force, force reactions on the skin surface, and the four load cells' measurements.

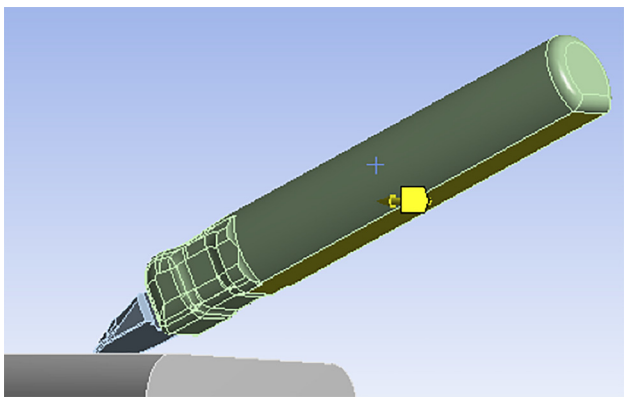

Fig. 11 The QSTM device movement constraint area in ANSYS

Four faces of the QSTM's head and the upper side of the arm section model were selected to be the contact areas, as shown in Fig. 10. Using Eq. (1), the augmented Lagrange formulation was enabled, and λ reduced the solution sensitivity to the contact stiffness[3]

$$F_{\text{normal}} = k_{\text{normal}} x_{\text{penetration}} + \lambda \tag{1}$$

Using ANSYS WORKBENCH R15.0 tools, the initial contact data were achieved and analyzed. The workbench provides simulation connections, penetration, geometrics' gap, and the pinballs' radii, that insure of an accurate connection solving. It differentiates the far and close connection areas while targeting the predicted connection elements [6].

In terms of movement constraint, the device's bottom was chosen to perform the displacement constraint, as shown in Fig. 11. The device was allowed to move into the skin's surface that expressed as the *Z* axis with respect to the QSTM device coordinate. However, side motions (*X*-axis) or vertical motions (*Y*-axis) were prohibited since this study investigated the straight strokes.

Different gripping styles played a role along with the hand placements during the IASTM. As shown in Figs. 12(*a*) and 12(*b*), force could be applied on the device's neck (pencil grip) or the device's back side. They would have achieved the same results if they had the same measured forces and angle. In this simulation, the back cover with an area of 207.14 mm^2 was selected to apply tabled compression forces in 12 s, as shown in Table 3. That resulted in good force convergence and reduced solving time.

Frictional Contact Between Tip and Skin. Frictional scenarios had similar simulation setup compared to the bonded scenario. These differences included the frictional contraction between the device's tip and the skin model, and the static structural and boundary conditions. In real IASTM practice, the tools slide over different areas of a human skin with the presence of gel, which reduces the friction. Stainless steel is a commonly used material in IASTM treatment. This connection was defined a frictional connection, despite the presence of the gel. The frictional coefficient is an important criterion to determine the type of friction between two materials. The friction coefficient represents the relationship between the friction forces and the normal reactions between two opposite surfaces. The friction coefficient, between an outer skin sample and the stainless steel, was found to be 1 [33]. As shown in Fig. 10, the four surfaces of the device's tip and the top surface of the skin model were selected to apply the friction coefficient.

[3]http://www.ansys.com

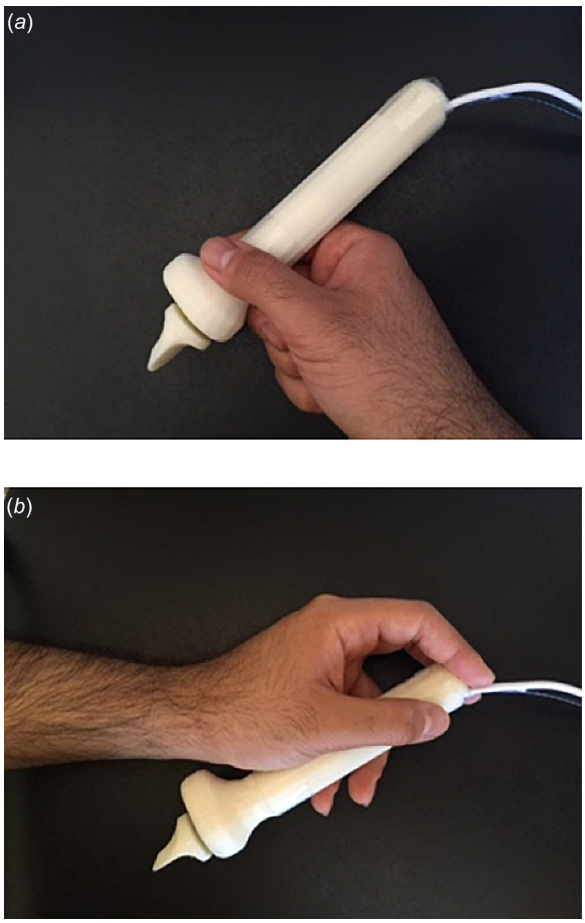

Fig. 12 (*a*) Pencil grip of QSTM device and (*b*) back cover grip of QSTM device

Table 3 Tabled hand forces (bonded contact)

Steps	Time (s)	Force (N)
1	0	10
	1	15
2	2	30
3	3	45
4	4	60
5	5	70
6	6	75
7	7	80
8	8	85
9	9	90
10	10	95
11	11	110
12	12	120

Table 4 Hand pressure applied to the QSTM device (frictional contact)

Steps	Time (s)	Pressure (MPa)
1	0	0
	1	0.1
2	2	
3	3	0.2
4	4	
5	5	
6	6	0.25
7	7	

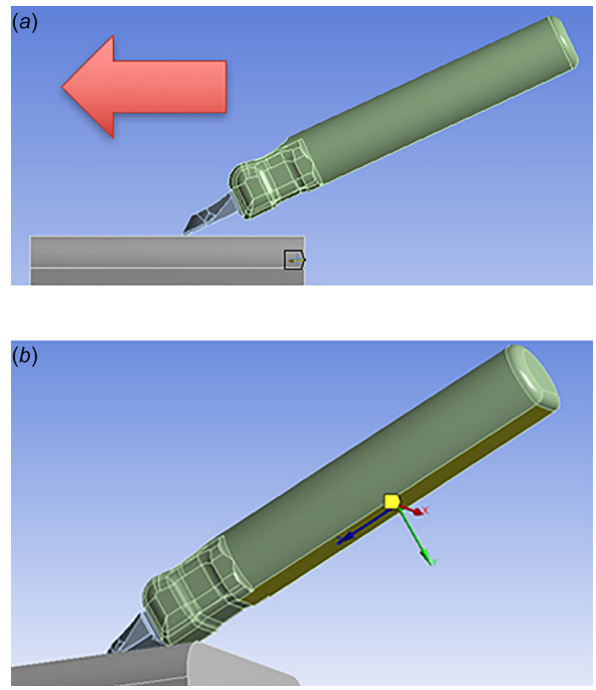

Fig. 13 (*a*) The QSTM device acceleration direction in ANSYS and (*b*) device displacement constraint areas in ANSYS

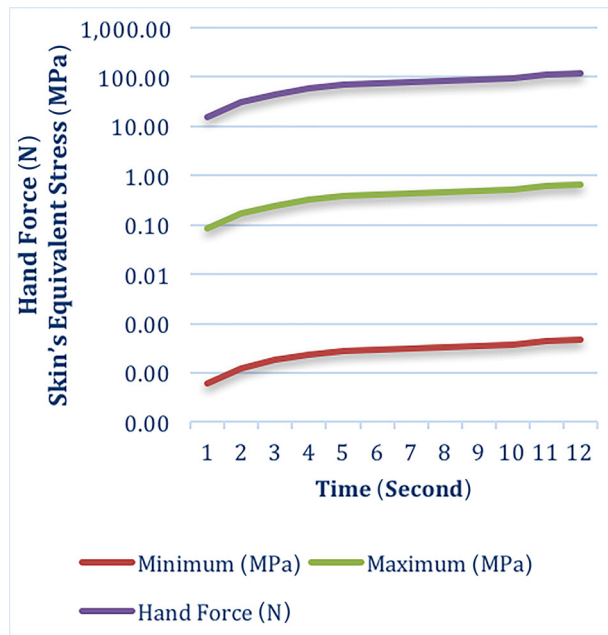

(*a*)

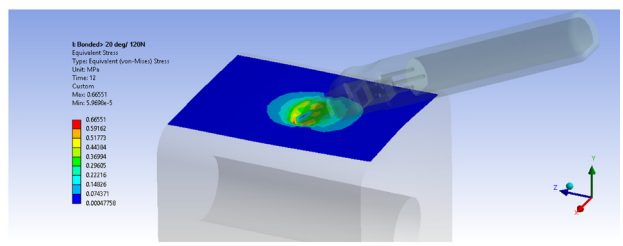

(*b*)

Fig. 14 Bonded connection results: (*a*) hand pressure versus skin's equivalent stress during 12 s finite element analysis (FEA) simulation and (*b*) skin's maximum equivalent stress at max hand force of 120 N in ANSYS

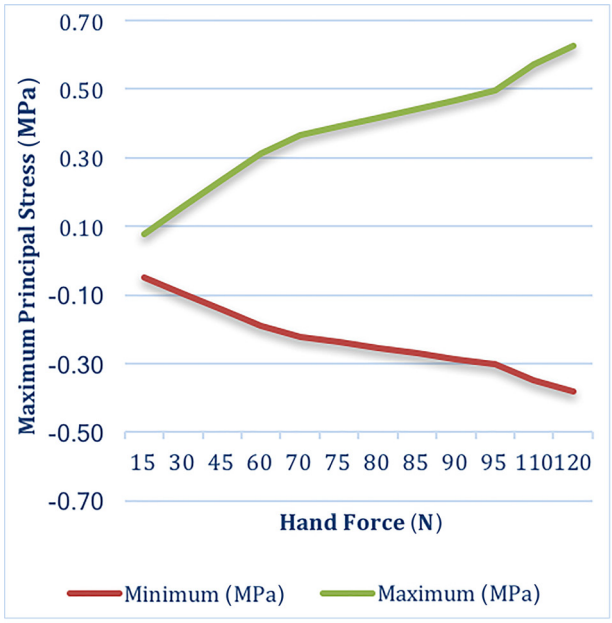

(*a*)

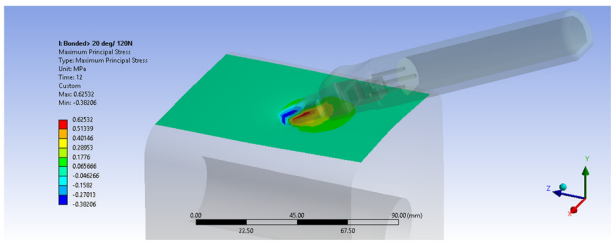

(*b*)

Fig. 15 Bonded connection results: (*a*) skin's maximum principal stress versus applied hand force and (*b*) maximum principal stress's maximum value of at hand force of 120 N in ANSYS

The simulation time was running for 6.3 s in seven steps. To assist the solution convergence, the Newton Raphson option was enabled. The device was set to accelerate with 0.5 mm/s^2 on the skin's surface, as shown in Fig. 13(*a*). This assumption was approximated by considering the actual practice of IASTM.

In terms of movement constraint, the device's bottom was chosen to perform the displacement constraint, as shown in Fig. 13(*b*). The device was allowed to move into the skin's surface that expressed as the *Z* axis in the QSTM device coordinate system. Similar to the real practice of IASTM, the QSTM device was appointed to accelerate with 0.5 mm/s^2 alongside the skin's surface model. However, side movements (*X*-axis) were prohibited since this study investigated the straight strokes. In this simulation, the back cover with an area of 207.14 mm^2 was selected to apply tabled compression forces, as shown in Table 4. This resulted in good force convergence and reduced solving time.

Simulation Results for Bonded Contact. The FEA was accomplished to investigate the pressure and deformation on the skin model and force measurements with respect to hand forces.

As shown in Fig. 14(*a*), the relation between the applied hand force and the von Mises stress (equivalent stress) on the skin model was obtained. Obviously, both minimum and maximum equivalent stresses on the skin increased when hand pressure increased. The maximum equivalent stress reached the maxima when hand force reached 120 N, as shown in Fig. 14(*b*). The base-10 logarithm for *y* axis was considered to show the complete variation. Almost zero minimum equivalent stress was recorded during the simulation run.

As shown in Fig. 15(*a*), the relation between the applied hand force and the maximum principal stress on the arm model was obtained. The maximum principal stress was used to assist the deterioration phase of the skin model. Obviously, both minimum (compression) and maximum (tension) maximum principal stresses on the arm increased when hand force increased. The maximum principal stress reached the maximum when hand force reached 120 N, as shown in Fig. 15(*b*). Since both maximum principal stresses did not reach the UTS of the skin model, the skin model would be safe under these force range.

Applying certain forces through the QSTM device would cause skin to deform. This deformation is a crucial character during the IASTM. Maximum and minimum values of skin deformation were recorded, as shown in Fig. 16(*a*). Both were proportional to the applied hand pressure; however, the maximum deformation was the highest during the simulation. As shown in Fig. 16(*b*), the maximum deformation of 9.2811 mm was recorded at hand force of 120 N, where the minimum deformation was 1.4865 mm. The

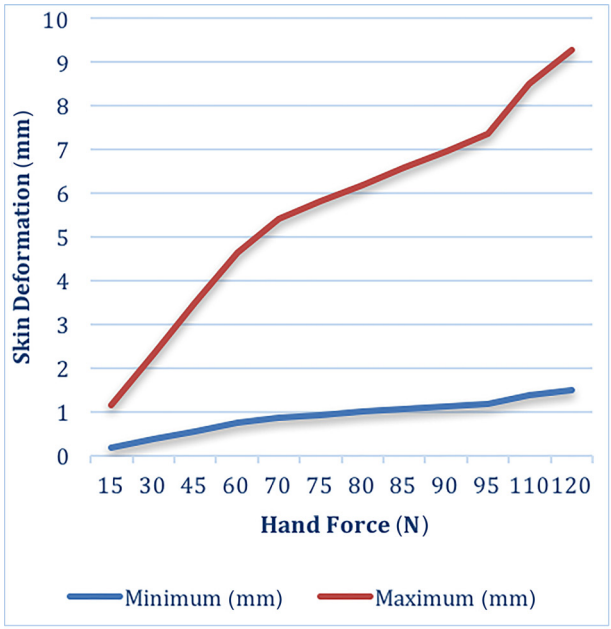

(*a*)

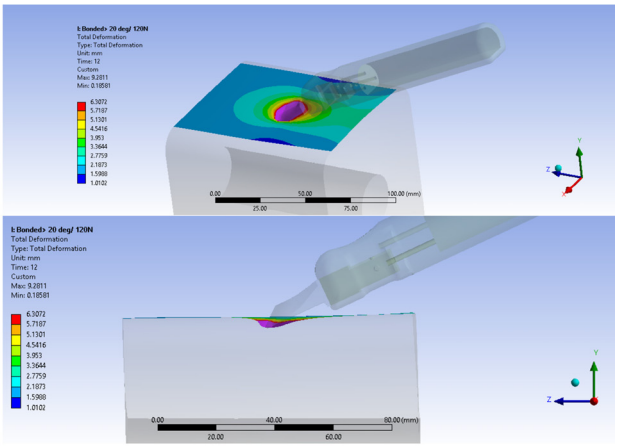

(*b*)

Fig. 16 Bonded connection results: (*a*) skin total deformation versus applied hand force and (*b*) skin's maximum deformation (9.2811 mm) where applied force 120 N in ANSYS

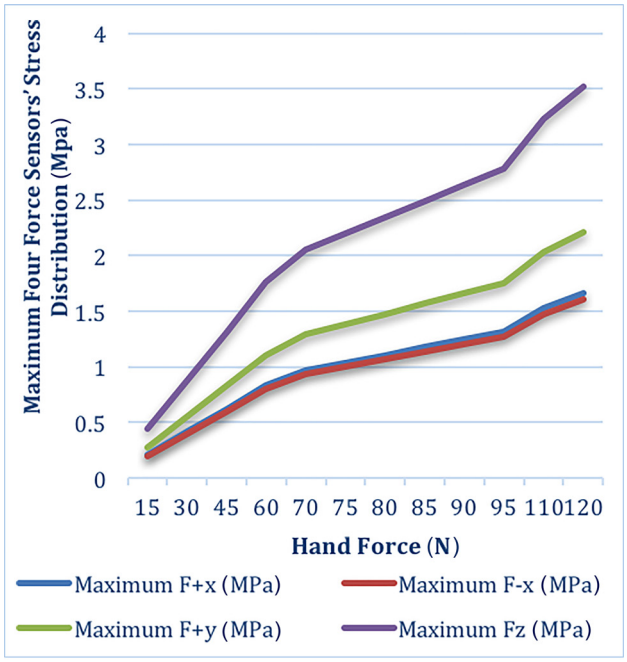

(*a*)

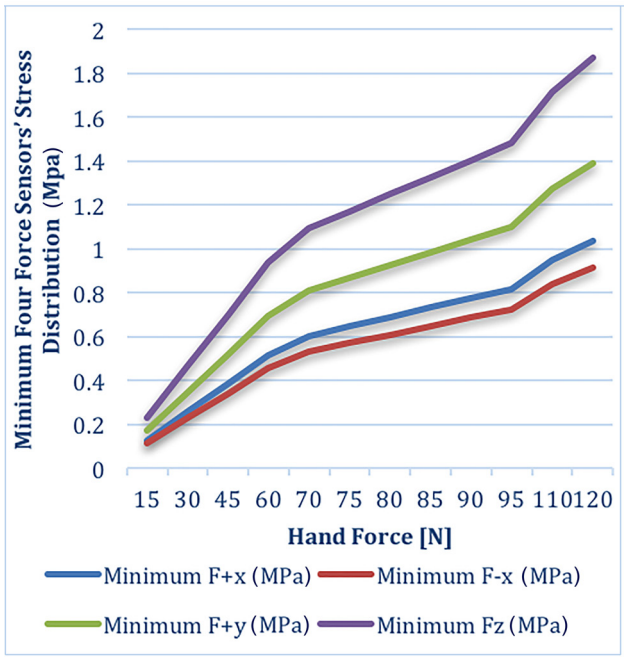

(*b*)

Fig. 17 Bonded connection results: maximum (*a*) and minimum (*b*) four force sensors' stress measurement versus hand force

minimum deformation recorded at the areas that are far from the device's interaction region.

The Resultant Force Measurements. The resultant force (stress) measurements on the load cells' tips were recorded in the QSTM device. As shown in Figs. 17(*a*) and 17(*b*), both maximum and minimum applied stresses distributed on the force sensors' tips with respect to the hand pressure were examined. The load cell's tips had a circular diameter of 2 mm^2. The load cells F_{+y} and F_Z were measuring greater stresses than the load cells on the X-axis. Based on the force vector analysis, a higher force/stress component was expected to be measured on F_{+y} and F_Z load cells. The highest measurement of those two load cells was dependent on the QSTM orientation angles (pitch), which was 20 deg in this simulation. As a result, the force sensor F_Z was recording the extremist maximum and minimum stresses distribution on the load cells' tip, and the force sensor was measuring a lower component $F_{+y.}$ than F_Z.

Simulation Results for Frictional Contact. The FEA was accomplished to investigate the pressure and deformation on the skin model and force measurements with respect to hand forces.

As shown in Fig. 18(*a*), the relation between the applied hand force and the von Mises stress (equivalent stress) on the skin model was obtained. Obviously, both minimum and maximum equivalent stresses on the skin increased when hand pressure increased. The maximum equivalent stress reached the maxima when hand pressure reached 0.20 MPa at 2.49 s, as shown in Fig. 18(*b*). Almost zero minimum equivalent stress was recorded during the simulation run since some areas of the skin model were barely stressed.

As shown in Fig. 19(*a*), the relation between the applied force and the maximum principal stress on the arm model was obtained. Obviously, both minimum (compression) and maximum (tension) principal stresses on the skin increased when hand force increased. The maximum principal stress reached the maxima at the skin's compressed areas when a hand force of 0.25 MPa was applied, as shown in Fig. 19(*b*). The compression maximum principal stress was higher than tension during the simulation due to the intention of the skin model to tear under the compression force more than tension. The

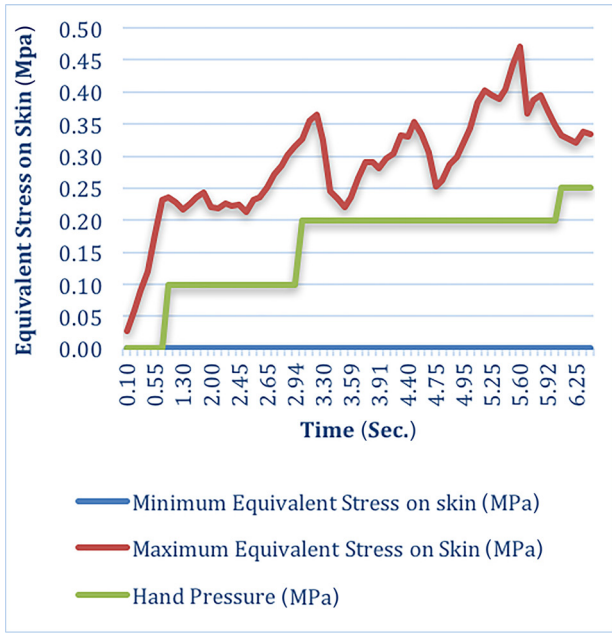

(*a*)

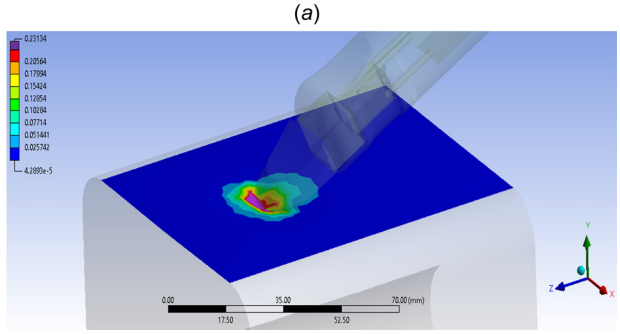

(*b*)

Fig. 18 Frictional connection results: (*a*) hand force versus skin's equivalent stress during 6.25 s and (*b*) the greatest maximum equivalent stress at hand force of 0.20 MPa in ANSYS

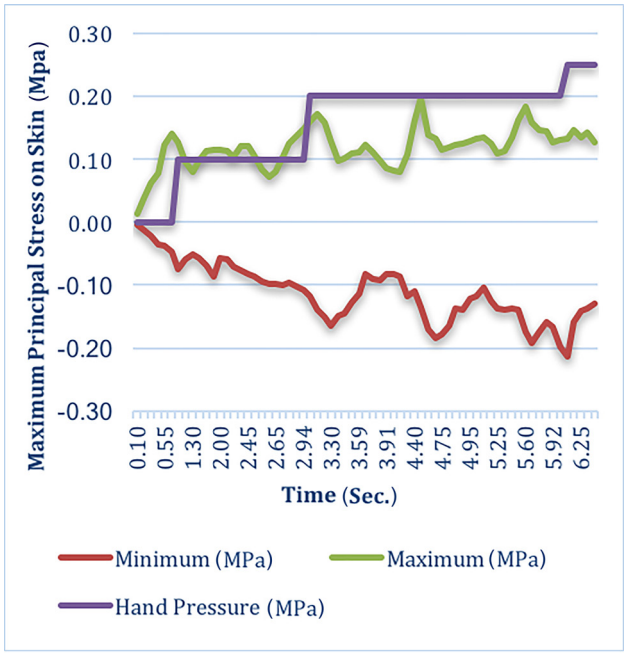

(*a*)

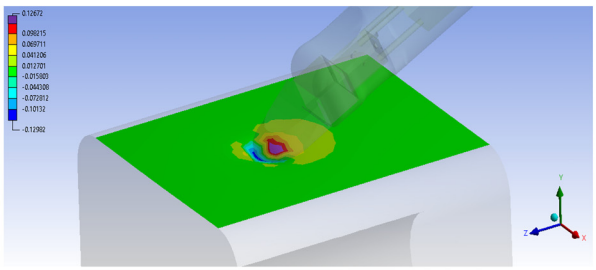

(*b*)

Fig. 19 Frictional connection results: (*a*) skin's maximum principal stress versus hand pressure during 6.25 s and (*b*) the maxima of the maximum principal stress at hand force of 0.25 MPa (frictional connection) in ANSYS

maximum principal stresses did not reach the UTS of the skin model, the skin model would be safe under this pressure range.

In terms of skin model deformation, maximum and minimum values of skin deformation were recorded, as shown in Fig. 20(*a*). Both were proportional to the applied hand pressure; however, the maximum deformation was the highest during the simulation. As shown in Fig. 20(*b*), the maximum deformation of 4.0012 mm was found at hand force of 0.25 MPa, where the minimum deformation was 0.18247 mm. The minimum deformation recorded at the areas that are far from interaction regain between the skin model and the QSTM device.

The Resultant Force Measurements. The resultant pressure (stress) measurements on the load cells' tips were recorded in the QSTM device. As shown in Figs. 21(*a*) and 21(*b*), both maximum and minimum applied stress distributions on the force sensors' tip with respect to the hand pressure were examined. The load cell's tips had a circular diameter of 2 mm^2. The force sensors F_{+y} and F_Z were measuring greater stresses than the load cells on the *X*-axis. Since the QSTM device was tilted with an angle of 20 deg, the load cell F_z was recording the greatest maximum and minimum stresses distribution on the load cells' tip. Also, the load cell F_{+y} was measuring a relatively smaller force component than F_z until the hand force increased to 0.20 MPa, where the arm's upper surface deformation was 2.8566 mm.

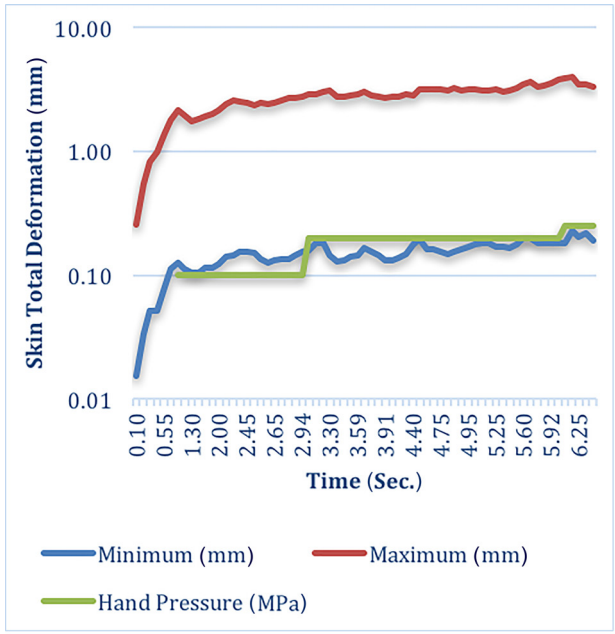

(*a*)

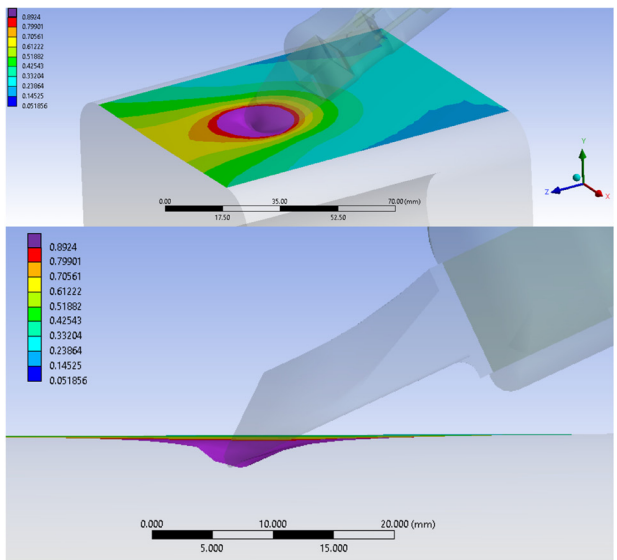

(*b*)

Fig. 20 Frictional connection results: (*a*) skin model deformation under hand pressure during 6.25 s and (*b*) skin maximum deformation (4.0012 mm) at hand force of 0.25 MPa in ANSYS

In terms of the minimum stresses, the stress distribution on F_{+y} and F_Z load cells were the highest; in other words, they measured the highest force components during the simulation. However, the load cell F_{+y} started measuring a higher force component than F_Z when applied hand force increased to 0.20 MPa, as shown in Fig. 21(*b*). This would not affect the measurement since the force analysis agreed with the load cells reading in the case of maximum stress distributions on the load cells.

In terms of the stress distribution on the load cells' tips, the load cells S_z and S_{+y} proved their functionality to measure the force components on these directions when the device moved longitudinally along the skin surface (as simulated). Finally, the load cell S_{-y} was able to be eliminated based on the force factorization that has been performed in the beginning of the study. This will reduce the final product price and the electronics needed for signal filtering.

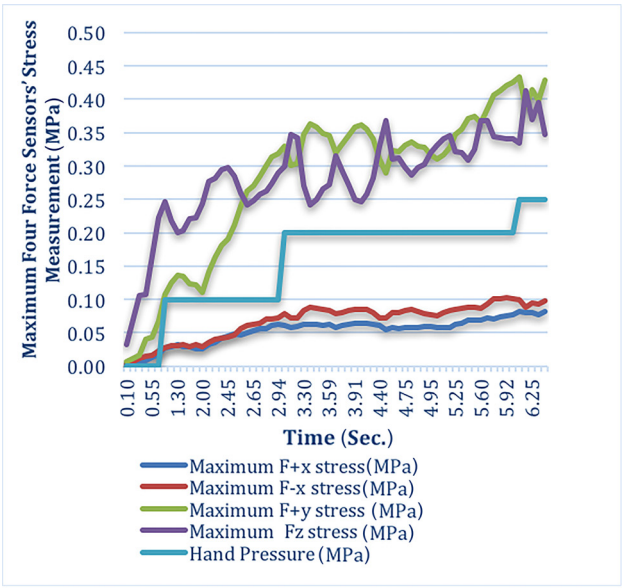

(*a*)

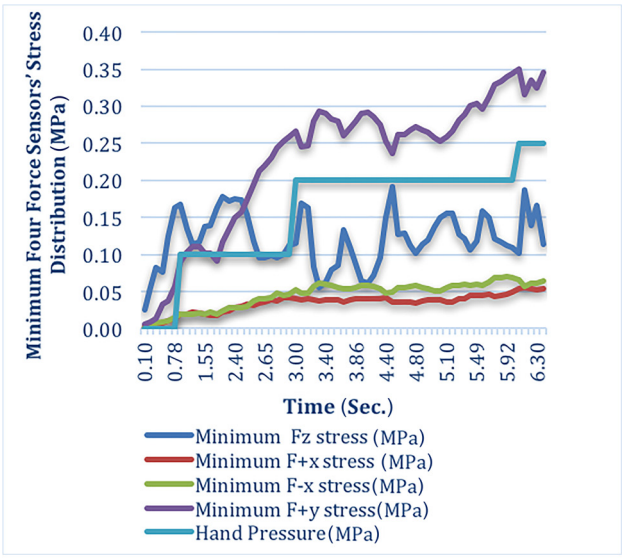

(*b*)

Fig. 21 Frictional connection results: maximum (*a*) and minimum (*b*) four force sensors' stress distribution versus hand pressure during 6.25 s

Conclusion

Instrument-assisted soft tissue manipulation is a style of physical therapy treatment utilizing a solid tool. The applied force to a patient in IASTM has not been quantified precisely for standardized clinical and research purposes. In this study, a novel mechatronic IASTM device (QSTM) was conceived, analyzed, and tested using FEA. Stress/strain distribution on a human arm model against hand pressure was simulated using the proposed QSTM device. A simplified human arm was modeled to investigate the relationship between the measured component forces, the applied force, and the stress and strain distribution on the skin surface to validate the capability of the QSTM instrument. The results show that the QSTM instrument as designed is able to correlate the measured force components to the applied tool-tip force in a straight movement on the skin model. Based on force factorization of the practice, it was found that four 1D compression load cells are sufficient to quantify the delivered force at the tool tip-skin interface. The analysis showed that a fifth load cell was not needed in the direction of $Y-$ which would reduce the final cost of the new QSTM device. The load cells S_z and S_{+y} have measured at the highest force components when the device moved longitudinally along the skin surface. Readily available, cost-effective QSTM will advance the field of physical therapeutics.

Further work will concentrate on investigating other scenarios, e.g., arch trajectory movements and more realistic relationship between the device's tip and the arm model as well as that between the QSTM tip and body. Also, inclusion of the transverse measurements on the X-axis and momentary effects on skin surface will be studied.

Nomenclature

S_{x-} = sensor (load cell) in the $X-$ direction
S_{x+} = sensor (load cell) in the $X+$ direction
S_{y+} = sensor (load cell) in the $Y+$ direction
S_{z+} = sensor (load cell) in the $Z+$ direction

References

[1] Kumar, S., Beaton, K., and Hughes, T., 2013, "The Effectiveness of Massage Therapy for the Treatment of Nonspecific Low Back Pain: A Systematic Review of Systematic Reviews," Int. J. Gen. Med., **6**, pp. 733–741.

[2] Crane, J. D., Ogborn, D. I., Cupido, C., Melov, S., Hubbard, A., Bourgeois, J. M., and Tarnopolsky, M. A., 2012, "Massage Therapy Attenuates Inflammatory Signaling After Exercise-Induced Muscle Damage," Sci. Transl. Med., **4**(119), pp. 13–119.

[3] Best, T. M., Crawford, S. K., Haas, C., Charles, L., and Zhao, Y., 2014, "Transverse Forces in Skeletal Muscle With Massage-Like Loading in a Rabbit Model," BMC Complementary Altern. Med., **14**(1), p. 393.

[4] Davidson, C. J., Ganion, L. R., Gehlsen, G. M., Verhoestra, B., Roepke, J. E., and Sevier, T. L., 1997, "Rat Tendon Morphologic and Functional Changes Resulting From Soft Tissue Mobilization," Med. Sci. Sports Exercise, **29**(3), pp. 313–319.

[5] Gehlsen, G. M., Ganion, L. R., and Helfst, R., 1999, "Fibroblast Responses to Variation in Soft Tissue Mobilization Pressure," Med. Sci. Sports Exercise, **31**(4), pp. 531–535.

[6] Loghmani, M. T., and Warden, S. J., 2009, "Instrument-Assisted Cross Fiber Massage Accelerates Knee Ligament Healing," J. Orthop. Sports Phys. Ther., **39**(7), pp. 506–514.

[7] Loghmani, M. T., and Warden, S. J., 2013, "Instrument-Assisted Cross Fiber Massage Increases Tissue Perfusion and Alters Microvascular Morphology in the Vicinity of Healing Knee Ligaments," BMC Complementary Altern. Med., **13**(1), p. 240.

[8] Looney, B., Srokose, T., Fernandez-De-Las-Peas, C., and Cleland, J. A., 2011, "Graston Instrument Soft Tissue Mobilization and Home Stretching for the Management of Plantar Heel Pain: A Case Series," J. Manipulative Physiol. Ther., **34**(2), pp. 138–142.

[9] Bayliss, A. J., Klene, F. J., Gundeck, E. L., and Loghmani, M. T., 2011, "Treatment of a Patient With Post-Natal Chronic Calf Pain Utilizing Instrument-Assisted Soft Tissue Mobilization: A Case Study," J. Man. Manipulative Ther., **19**(3), pp. 127–134.

[10] McCrea, E. C., and George, S. Z., 2010, "Outcomes Following Augmented Soft Tissue Mobilization for Patients With Knee Pain: A Case Series," Orthop. Phys. Ther. Pract., **22**(2), pp. 69–74.

[11] Burke, J., Buchberger, D. J., Carey-Loghmani, M. T., Dougherty, P. E., Greco, D. S., and Dishman, J. D., 2007, "A Pilot Study Comparing Two Manual Therapy Interventions for Carpal Tunnel Syndrome," J. Manipulative Physiol. Ther., **30**(1), pp. 50–61.

[12] Phipps, R. L., Carney, S. R., Loghmani, M. T., and Bayliss, A. J., 2011, "An Innovative Manual Therapy Approach for the Treatment of Patients With Achilles Tendinopathy: A Case Series," J. Orthop. Sports Phys. Ther., **41**(1), pp. A65–A66.

[13] Heinecke, M. L., Thuesen, S. T., and Stow, R. C., 2014, "Graston Technique on Shoulder Motion Graston Technique on Shoulder Motion in Overhead Athletes," J. Undergrad. Kinesiology Res., **1**(10), pp. 27–39.

[14] Laudner, K., Compton, B. D., McLoda, T. A., and Walters, C. M., 2014, "Acute Effects of Instrument Assisted Soft Tissue Mobilization for Improving Posterior Shoulder Range of Motion in Collegiate Baseball Players," Int. J. Sports Phys. Ther., **9**(1), pp. 1–7.

[15] Terry Loghmani, M., Bayliss, A. J., Clayton, G., and Gundeck, E., 2015, "Successful Treatment of a Guitarist With a Finger Joint Injury Using Instrument-Assisted Soft Tissue Mobilization: A Case Report," J. Man. Manipulative Ther., **23**(5), pp. 246–253.

[16] Black, P., 2010, "Treatment of Knee Arthrofibrosis and Quadriceps Insufficiency After Patellar Tendon Repair: A Case Report Including Use of the Graston Technique," IJTMB, **3**(2), pp. 14–21.

[17] Lee, H. M., Wu, S. K., and You, J. Y., 2009, "Quantitative Application of Transverse Friction Massage and Its Neurological Effects on Flexor Carpi Radialis," Man. Ther., **14**(5), pp. 501–507.

[18] Wang, Q., Zeng, H., Best, T. M., Haas, C., Heffner, N. T., Agarwal, S., and Zhao, Y., 2014, "A Mechatronic System for Quantitative Application and Assessment of Massage-like Actions in Small Animals," BMES, **42**(1), pp. 36–49.
[19] Sherman, K., Cook, A., Kahn, J., Hawkes, R., Wellman, R., and Cherkin, D., 2017, "Dosing Study of Massage for Chronic Neck Pain: Protocol for the Dose Response Evaluation and Analysis of Massage [DREAM] Trial," BMC Complementary Altern. Med., **12**(1), pp. 1–16.
[20] Sherman, K., Cook, A., Wellman, R., Hawkes, R., Kahn, J., Deyo, R., and Cherkin, D., 2017, "Five-Week Outcomes From a Dosing Trial of Therapeutic Massage for Chronic Neck Pain," Ann. Family Med., **12**(2), pp. 112–120.
[21] Cook, A., Wellman, R., Cherkin, D., Kahn, J., and Sherman, K., 2015, "Randomized Clinical Trial Assessing Whether Additional Massage Treatments for Chronic Neck Pain Improve 12- and 26-Week Outcomes," Spine J., **15**(10), pp. 2206–2215.
[22] Haas, C., Butterfield, T., Zhao, Y., Zhang, X., Jarjoura, D., and Best, T., 2012, "Dose-Dependency of Massage-Like Compressive Loading on Recovery of Active Muscle Properties Following Eccentric Exercise: Rabbit Study With Clinical Relevance," Br. J. Sports Med., **47**(2), pp. 83–88.
[23] Haas, C., Butterfield, T., Abshire, S., Zhao, Y., Zhang, X., Jarjoura, D., and Best, T., 2013, "Massage Timing Affects Postexercise Muscle Recovery and Inflammation in a Rabbit Model," Med. Sci. Sports Exercise, **45**(6), pp. 1105–1112.
[24] Haas, C., Best, T., Wang, Q., Butterfield, T., and Zhao, Y., 2012, "In Vivo Passive Mechanical Properties of Skeletal Muscle Improve With Massage-Like Loading Following Eccentric Exercise," J. Biomech., **45**(15), pp. 2630–2636.
[25] Butterfield, T., Zhao, Y., Agarwal, S., Haq, F., and Best, T., 2008, "Cyclic Compressive Loading Facilitates Recovery After Eccentric Exercise," Med. Sci. Sports Exercise, **40**(7), pp. 1289–1296.
[26] Zeng, H., Butterfield, T., Agarwal, S., Haq, F., Best, T., and Zhao, Y., 2008, "An Engineering Approach for Quantitative Analysis of the Lengthwise Strokes in Massage Therapies," ASME J. Med. Dev., **2**(4), p. 041003.
[27] Femto.io, 2016, "IMUduino," Femto.io, American Canyon, CA, accessed Apr. 12, 2018, https://femtoduino.com/shop
[28] Forsentek, 2016, "Micro Compression Load Cell Force Sensor," Forsentek, Shenzhen, China, accessed Apr. 14, 2018, http://www.forsensor.com/
[29] Agache, P. G., Monneur, C., Leveque, J. L., and De Rigal, J., 1980, "Mechanical Properties and Young's Modulus of Human Skin In Vivo," Arch. Dermatol. Res., **269**(3), pp. 221–232.
[30] Elert, G., 1998, "The Physics Hypertextbook, Vol. 9," hypertextbook.com, Brooklyn, NY, accessed Feb. 21, 2016, http://physics.info
[31] Delalleau, A., Josse, G., Lagarde, J., Zahouani, H., and Bergheau, J., 2006, "Characterization of the Mechanical Properties of Skin by Inverse Analysis Combined With the Indentation Test," J. Biomech., **39**(9), pp. 1603–1610.
[32] Gallagher, A. J., Ní Annaidh, A., and Bruyère, K., 2012, "Dynamic Tensile Properties of Human Skin," International Research Council on the Biomechanics of Injury Conference (IRCOBI), Dublin, Ireland, Sept. 12–14, pp. 494–502.
[33] Veijgen, N., Masen, M., and van der Heide, E., 2012, "A Novel Approach to Measuring the Frictional Behaviour of Human Skin In Vivo," Tribol. Int., **54**, pp. 38–41.